

## Measurements of Phase Dynamics in Planar Josephson Junctions and SQUIDs

D. Z. Haxell,<sup>1</sup> E. Cheah<sup>2</sup>, F. Křížek<sup>1,2</sup>, R. Schott<sup>2</sup>, M. F. Ritter,<sup>1</sup> M. Hinderling,<sup>1</sup> W. Belzig<sup>3</sup>, C. Bruder,<sup>4</sup>  
W. Wegscheider,<sup>2</sup> H. Riel,<sup>1</sup> and F. Nichele<sup>1,\*</sup>

<sup>1</sup>IBM Research Europe—Zurich, Säumerstrasse 4, 8803 Rüschlikon, Switzerland

<sup>2</sup>Solid State Physics Laboratory, ETH Zurich, 8093 Zurich, Switzerland

<sup>3</sup>Fachbereich Physik, Universität Konstanz, D-78457 Konstanz, Germany

<sup>4</sup>Department of Physics, University of Basel, Klingelbergstrasse 82, CH-4056 Basel, Switzerland



(Received 12 April 2022; revised 15 September 2022; accepted 19 January 2023; published 23 February 2023)

We experimentally investigate the stochastic phase dynamics of planar Josephson junctions (JJs) and superconducting quantum interference devices (SQUIDs) defined in epitaxial InAs/Al heterostructures, and characterized by a large ratio of Josephson energy to charging energy. We observe a crossover from a regime of macroscopic quantum tunneling to one of phase diffusion as a function of temperature, where the transition temperature  $T^*$  is gate-tunable. The switching probability distributions are shown to be consistent with a small shunt capacitance and moderate damping, resulting in a switching current which is a small fraction of the critical current. Phase locking between two JJs leads to a difference in switching current between that of a JJ measured in isolation and that of the same JJ measured in an asymmetric SQUID loop. In the case of the loop,  $T^*$  is also tuned by a magnetic flux.

DOI: [10.1103/PhysRevLett.130.087002](https://doi.org/10.1103/PhysRevLett.130.087002)

Two-dimensional superconductor-semiconductor hybrid systems are a promising platform for scalable quantum computation and for the study of novel physical phenomena. The possibility to produce transparent interfaces [1–9], combined with flexible lithographic patterning, is paving the way to a new generation of voltage-tunable qubit architectures [10–16], with planar Josephson junctions (JJs) and superconducting quantum interference devices (SQUIDs) as core elements. Furthermore, spin-orbit interaction and Zeeman fields enable a rich playground for fundamental physics [17–19], including the realization of topological states of matter [20–25]. In this context, understanding the phase dynamics of hybrid JJs and SQUIDs, which ultimately determine their switching currents, is crucial.

Here we investigate the stochastic phase dynamics of hybrid JJs defined in an InAs/Al planar heterostructure [3]. We show that macroscopic quantum tunneling (MQT) and phase diffusion (PD) are the most relevant phase escape regimes. The low-temperature mean switching current  $I_M$  is a small fraction of the critical current  $I_C$ , although the Josephson energy  $E_J$  is significantly larger than the charging energy  $E_C$ . In JJs with small  $I_C$ , the suppression of  $I_M$  is strong enough that PD dominates at low

temperature. Embedding a JJ in an asymmetric SQUID, an approach intensively pursued for realizing topological states [22–25], modifies the phase escape mechanism. Thus,  $I_M$  may significantly vary when a JJ is measured in isolation or in a SQUID (by a factor of approximately 2.5, in the present case). The dominant phase-escape mechanism is further tuned via temperature, gate voltages, and fluxes threading the SQUID. Contrary to conventional metallic JJs, no indication of thermal phase activation is observed. Characteristic experimental features are reproduced with a Monte Carlo simulation of the phase dynamics. Our results indicate that phase dynamics significantly affect the switching current of hybrid devices, and guide towards the realization of novel quantum architectures.

Figure 1(a) shows a micrograph of the device under study. It consists of two gate-tunable planar JJs (JJ1 and JJ2) embedded in a SQUID loop, all defined in an InAs quantum well (pink) covered by a thin layer of *in situ*-deposited Al (blue) [3]. Devices were defined by wet etching of the Al, followed by deposition of a 15 nm HfO<sub>x</sub> layer and metallic gates (yellow). Gate voltages  $V_{G1}$  and  $V_{G2}$  allowed tuning of JJ1 and JJ2, respectively. The gate voltage  $V_{\text{Global}}$  was kept constant at  $-600$  mV to prevent parallel conduction in the semiconductor. The design was optimized to reach a critical current in JJ1 ( $I_{C,1}$ ) that was much larger than the critical current in JJ2 ( $I_{C,2}$ ) [22,26]. This was achieved by changing the lateral extent of the Al electrodes ( $5 \mu\text{m}$  in JJ1 vs  $1.6 \mu\text{m}$  in JJ2) and their separation ( $50$  nm in JJ1 vs  $100$  nm in JJ2). Electronic measurements were conducted in a dilution refrigerator

Published by the American Physical Society under the terms of the [Creative Commons Attribution 4.0 International license](https://creativecommons.org/licenses/by/4.0/). Further distribution of this work must maintain attribution to the author(s) and the published article's title, journal citation, and DOI.

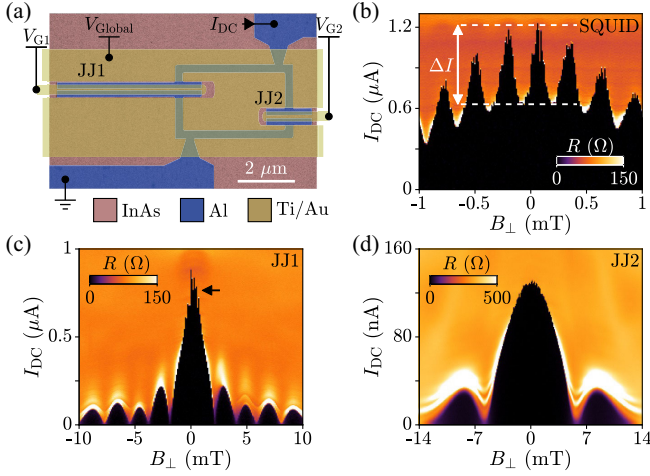


FIG. 1. (a) False-colored electron micrograph of the device under study and measurement configuration. The InAs is highlighted in pink and the Al in blue. Gates are drawn on the image and highlighted in yellow. (b) Differential resistance  $R$  as a function of  $B_{\perp}$  and  $I_{DC}$  obtained with  $V_{G1} = -180$  mV and  $V_{G2} = -140$  mV. The amplitude of the switching current oscillations,  $\Delta I$ , is marked. (c) Differential resistance of JJ1 in isolation, with  $V_{G1} = -180$  mV and  $V_{G2} = -450$  mV. Large fluctuations close to  $B_{\perp} = 0$  are marked with an arrow. (d) Differential resistance of JJ2 in isolation, with  $V_{G1} = -550$  mV and  $V_{G2} = -140$  mV. The peak at  $B_{\perp} = 0$  is less than half  $\Delta I/2$  in (b).

with a mixing chamber base temperature below 20 mK. Results presented here were confirmed on a second SQUID device and on several individual JJs.

We first present switching currents obtained with low-frequency lock-in techniques, similar to previous work [18,22,26]. A source-drain current  $I_{DC}$  was swept over timescales of seconds, while the SQUID differential resistance  $R$  was recorded. Figure 1(b) shows  $R$  as a function of out-of-plane magnetic field  $B_{\perp}$  with  $V_{G1} = -180$  mV and  $V_{G2} = -140$  mV, where  $I_{C,1}$  and  $I_{C,2}$  were independently maximized. The SQUID switching current  $I$  had a periodicity of 350  $\mu$ T, corresponding to a flux  $h/2e$  threading the loop. The amplitude of the SQUID oscillations,  $\Delta I$ , reveals the switching current of JJ2 as  $I_2 = \Delta I/2 = 350$  nA, while the mean value gives the switching current of JJ1,  $I_1 = 850$  nA. Figure 1(c) shows  $R$  when JJ2 is closed and with JJ1 in the gate configuration of Fig. 1(b). The Fraunhofer interference pattern emerges [27], with a maximum of  $I_1$  matching the mean switching current of Fig. 1(b). Furthermore, large switching current fluctuations were present at  $B_{\perp} = 0$  (black arrow). Figure 1(d) shows similar measurements performed with  $I_{DC}$  flowing in JJ2 only. Surprisingly, the maximum of  $I_2$  is 120 nA; a significant difference with the 350 nA deduced from Fig. 1(b).

Both the fluctuations in Fig. 1(c) and the switching current enhancement in Fig. 1(b) with respect to Fig. 1(d) are manifestations of the phase dynamics in our devices.

Therefore, we evaluate the phase escape mechanisms in JJ1 and JJ2 separately (Fig. 2), and in the SQUID loop formed by their combination (Fig. 3). Finally, we demonstrate gate and flux tunability of the escape dynamics (Fig. 4). To capture the stochastic characteristics of phase escape, we modulate the input current with a sawtooth function using a ramp rate  $\nu = 240 \mu\text{As}^{-1}$  and monitor the voltage across the SQUID with an oscilloscope. This technique allows us to record the switching current  $I_{SW}$  for 10 000 switching events in approximately ten minutes, and produce the switching probability distribution (SPD), that is the probability for a switch to occur per unit of input current. Similar techniques were used for detailed studies of conventional [28,29] and hybrid JJs [30–33], metallic nanowires [34–36], and SQUIDs [37–41].

Figures 2(a) and 2(b) show the SPDs of JJ1 and JJ2, respectively, measured at various mixing chamber temperatures  $T$ . The corresponding escape rates  $\Gamma$ , computed as [42]

$$\Gamma(I_{SW}) = \text{SPD}(I_{SW})\nu \left[ 1 - \int_0^{I_{SW}} \text{SPD}(I) dI \right]^{-1}, \quad (1)$$

are shown in Fig. 2(b) and 2(d), respectively.

Figures 2(e) and 2(f) show the mean value of the SPDs in JJ1 ( $I_{M,1}$ ) and its standard deviation ( $\sigma_1$ ), respectively, both as a function of  $T$ . For  $T < 400$  mK,  $\sigma_1$  is constant and large, and  $\Gamma$  increases exponentially with  $I_{SW}$ , indicating that MQT dominates the phase dynamics. For higher  $T$ ,  $\sigma_1$  decreases as  $T$  increases, signaling the crossover to PD, where escape and retrapping events have similar probabilities to occur, so that many escape events are required to transition to the resistive state. The temperature  $T^* \sim 0.55$  K marks the crossover between a regime dominated by MQT and one dominated by PD. Regimes with  $\sigma_1$  increasing with  $T$ , which indicate thermal activation (TA), were not observed. The width of the low-temperature SPD, expressed as  $\sigma/I_1 = 0.058$ , is particularly large and results in pronounced switching current fluctuations, as seen in the measurements of Fig. 1(c) (black arrow). Broad SPDs at low  $T$ , together with the absence of an intermediate TA regime, which is unusual in conventional JJs [43], indicate a large critical current  $I_{C,1}$  and a small capacitance  $C$  for JJ1. Finally, the relevance of PD, together with measuring a finite resistance at  $I_{DC} = 0$  for  $T > 1$  K, which is well below the critical temperature  $T_C$  of the Al [44], indicates moderate damping.

The temperature dependence of  $I_{M,1}$  and  $\sigma_1$  is well captured by a Monte Carlo simulation of the phase dynamics [gray line in Figs. 2(e) and 2(f)] [51], an approach previously adopted for the study of moderately damped JJs [52,53]. In particular, the capacitance  $C$  and the zero-temperature critical current  $I_{C,1}$  of JJ1 are first obtained by comparing the low-temperature data to a model of MQT. The quality factor  $Q_0$  is subsequently determined by comparing the full temperature dependence to the Monte Carlo simulation. Details on our

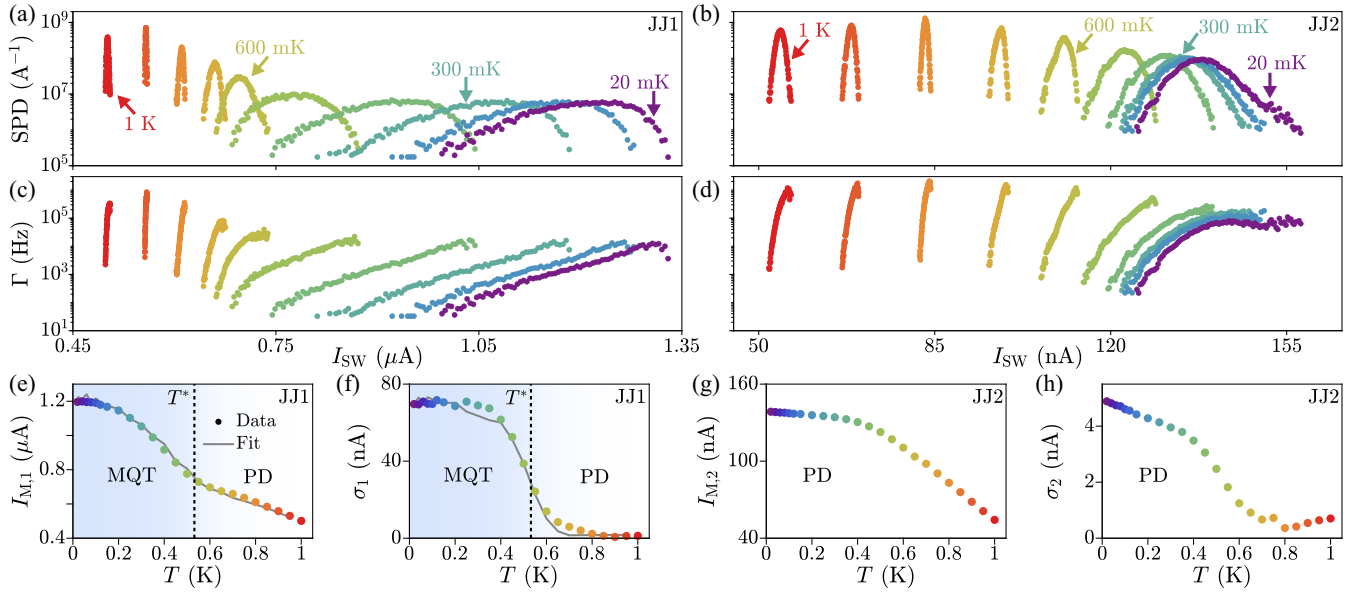


FIG. 2. (a) Switching probability distributions (SPDs) for JJ1 for various temperatures. Colors are defined in (e) and are consistent throughout the text. (b) As in (a), but for JJ2. (c) Escape rate  $\Gamma$  of JJ1, obtained from the data in (a) using Eq. (1). (d) As in (c), but for JJ2. (e) Mean switching current  $I_{SW}$  of SPDs for JJ1 as a function of temperature (circles) together with a fit to a Monte Carlo simulation (line). Transition temperature  $T^*$  is indicated by a vertical line, dividing a regime of MQT (blue shading) and PD. (f) Standard deviation  $\sigma_1$  of SPDs for JJ1, as a function of temperature. (g),(h) As in (e) and (f), for JJ2.

procedure are discussed in the Supplemental Material [44]. While this model was developed for tunneling JJs with sinusoidal current-phase relation and large  $Q_0$ , in the absence of a more complete theory, we tentatively apply it to our devices and consider the results to be of qualitative nature. The best fit was obtained with  $C = 1$  fF,  $I_{C,1} = 3$   $\mu$ A and  $Q_0 = 7$ . As expected, JJ1 is moderately damped and has a small intrinsic capacitance, leading to a large plasma frequency. The estimated  $I_{C,1}$  is 2.5 times higher than  $I_{M,1}$ , indicating that moderate input currents already result in a high switching probability. The ratio between  $I_{C,1}$  and  $I_{M,1}$  decreases towards one for  $T > T^*$ , as signaled by the kink in  $I_{M,1}$  at  $T = T^*$ . The result  $C = 1$  fF is consistent with the geometrical capacitance between the Al electrodes [44]. With these parameters, we estimate  $E_J/E_C = 73$  at  $T = 20$  mK [44]. This situation is very different from a conventional metallic Josephson junction, where strong suppression of  $I_{SW}$  from  $I_C$  requires  $E_J/E_C \leq 1$  [54–56]. Because of the small  $C$  and large  $I_C$ , we estimate that the transition from MQT to TA would occur for  $T > T_C$  so that, in the entire PD regime, phase escape takes place via MQT [44].

Similar to JJ1, MQT is the dominant phase escape mechanism in JJ2. However, large dissipation results in a significant retrapping probability and places JJ2 in the PD regime down to base temperature. This is evident from  $I_{M,2}$  and  $\sigma_2$  shown in Figs. 2(g) and 2(h), respectively, where  $\sigma_2$  does not saturate for  $T \rightarrow 0$ , and from the deviation of  $\Gamma$  from an exponential in Fig. 2(d). The small  $I_{C,2}$  likely sets  $Q_0 \sim 1$ , which is outside the range of validity of our Monte Carlo simulations.

We now present the phase dynamics when both JJs are activated. Figures 3(a) and 3(b) show the mean,  $I_{M,S}$ , and standard deviation,  $\sigma_S$ , of each SPD obtained in the gate configuration of Fig. 1(b) as a function of  $B_\perp$  and  $T$  [57]. In Fig. 3(a), SQUID oscillations are clearly captured by  $I_{M,S}$ . In Fig. 3(b), the curves at low  $T$  have a large  $\sigma_S$ , independent of  $B_\perp$ . As  $T$  increases further,  $\sigma_S$  is modulated by  $B_\perp$  and ultimately becomes small and independent of  $B_\perp$ . In Fig. 3(c) we compare  $I_{M,2}$  [squares, as in Fig. 2(g)] to the half-amplitude of the oscillations in  $I_{M,S}$  (circles). In the absence of macroscopic quantum tunneling, the two quantities would coincide. Instead, we find a significant discrepancy, highlighted by green shading, which is large at low  $T$  and vanishes above  $T^*$  of JJ1. By tuning  $T^*$  via  $V_{G1}$ , we confirm that the enhancement of  $\Delta I_{M,S}/2$  with respect to  $I_{M,2}$  was always correlated to  $T^*$  in JJ1 [44]. The mean value of  $I_{M,S}$  matched  $I_{M,1}$  [44] and the mean of  $\sigma_S$ ,  $\langle \sigma_S \rangle$ , was similar to  $\sigma_1$  [Fig. 3(d)].

The results presented in Fig. 3 are intuitively understood by considering phase locking by the loop inductance. For JJ2 alone, phase escape is more likely at moderate currents compared to JJ1. Coupling JJ2 to JJ1 effectively realizes a new JJ with higher Josephson energy and similar phase dynamics to JJ1, so that the dominant switching mechanism is MQT and, consequently, the suppression of  $I_M$  is reduced. However, protection of  $I_{M,2}$  is maintained while JJ1 stays in the MQT regime ( $T < T^*$ ), where phase uncertainty is less than in the PD regime. Consistent with this interpretation, phase dynamics in the asymmetric SQUID configuration are well described by a Monte Carlo

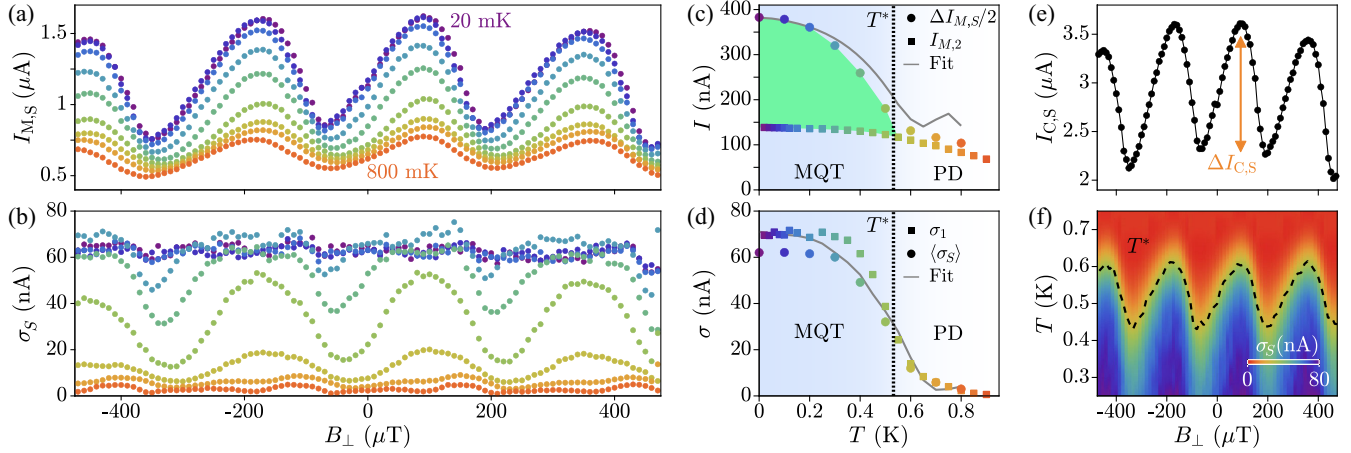


FIG. 3. Mean  $I_{M,S}$  (a) and standard deviation  $\sigma_S$  (b) of the SPDs in the SQUID configuration as a function of  $B_{\perp}$ , for temperatures between 20 and 800 mK. (c) Mean switching current of JJ2 as a function of  $T$ , derived from the SQUID oscillations (circles) and measured with JJ2 in isolation (squares). The solid line is  $\Delta I_{M,S}/2$  obtained from a Monte Carlo simulation fitted to the experimental results. (d) Standard deviation of the SPD in JJ1 measured in isolation (squares) together with the mean of  $\sigma_S$  from (b) (circles) as a function of temperature. The solid line is the result of the Monte Carlo simulation presented in (c). (e) SQUID critical current obtained by fitting the SPDs for  $T = 20$  mK to an MQT escape rate. (f) Color map of fitted standard deviation  $\sigma_S$ , with transition temperature  $T^*$  marked by a dashed line.

simulation of a fictitious JJ with a field-dependent critical current  $I_{C,S}(B_{\perp})$ , and with  $C$  and  $Q_0$  as derived for JJ1. The sole fit parameter was  $I_{C,S}$  for  $T = 20$  mK, which is shown in Fig. 3(e) as a function of  $B_{\perp}$  (circles). The curve is consistent with the presence of highly transmissive Andreev bound states (ABSs), resulting in a forward-skewed current-phase relation [26,58]. Also for the SQUID, the critical current  $I_{C,S}$  and mean switching current  $I_{M,S}$  [Fig. 3(a)] differ by a factor of approximately 2.5. After obtaining  $I_{C,S}(B_{\perp})$  for  $T = 20$  mK, the entire dataset of Figs. 3(a) and 3(b) was simulated without free parameters. We show the simulated half-amplitude  $\Delta I_{M,S}/2$  and the mean of  $\sigma_S$  as gray lines in Figs. 3(c) and 3(d), respectively. Despite the simplicity of our model, experimental results are reproduced to a large extent. Figure 3(f) shows a color map of the simulated standard deviation,  $\sigma_S(B_{\perp}, T)$ , with  $T^*$  indicated by a dashed line and marking the crossover between MQT and PD. The phase dynamics are completely described by MQT and PD for low and high  $T$ , respectively. For intermediate  $T$ , the phase escape mechanism periodically varies between MQT and PD as a function of  $B_{\perp}$ .

In the following, we discuss how phase escape dynamics vary as  $I_{C,1}$  and  $I_{C,2}$  are tuned via gate voltages. Figure 4(a) summarizes results for JJ2 as  $V_{G2}$  was varied. When JJ2 was measured in isolation, switching currents  $I_{M,2}$  were small, and PD was the dominant regime throughout the accessible range of  $V_{G2}$ . We highlight this condition with gray shading. When the SQUID was formed, the switching current of JJ2 deduced from the SQUID oscillations ( $\Delta I_{C,S}/2$ ) was significantly higher than when JJ2 was measured in isolation. We highlight this situation with green shading. For

$V_{G2} < 300$  mV JJ2 was resistive, if measured in isolation, presumably due to  $E_J/E_C \approx 1$  [54–56], but SQUID oscillations were still observed. Finally, the  $I_{C,2}$  obtained by fitting the SPDs in the SQUID with the Monte Carlo simulation [as in Fig. 3(e)] is highlighted in yellow.

Decreasing  $I_{C,1}$  via  $V_{G1}$  made the SQUID more symmetric and shifted JJ1 towards a regime of PD. Figures 4(b)–4(d) show  $\sigma_S$  for decreasing values of  $V_{G1}$ . For  $V_{G1} = -300$  mV and  $-350$  mV [Figs. 4(c) and 4(d), respectively] escape dynamics varied between MQT (blue shading) and PD already at base temperature, with  $\sigma_S$  oscillating between 10 and 60 nA within one SQUID

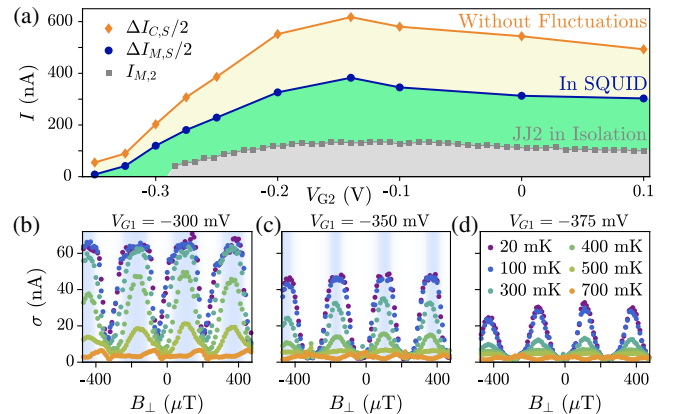


FIG. 4. (a) Switching currents of JJ2 as a function of  $V_{G2}$  when measured in isolation (squares) and in the SQUID configuration (circles), together with the critical current derived from Monte Carlo simulations (diamonds). (b)–(d) Standard deviation of SPDs measured in the SQUID configuration for three values of  $V_{G1}$ . Blue shading highlights MQT regimes.

oscillation. For  $V_{G1} = -375$  mV [Fig. 4(d)] PD dominated at low  $T$ , although modulations in  $\sigma_S$  persisted. Modeling the curves in Figs. 4(b)–4(d) would require a quantum treatment of the phase escape from a 2D potential, which goes beyond the scope of this Letter.

In conclusion, the switching current of planar JJs with highly transmissive ABSs is strongly affected by phase dynamics, even for  $E_J/E_C \gg 1$ . As a result of moderate dissipation ( $Q_0 < 10$ ) and large plasma frequency,  $I_M$  can differ largely from  $I_C$ , depending on the details of the JJs and of their electrostatic environment. Phase dynamics can be modified by embedding JJs in asymmetric SQUID geometries, resulting in significant changes of  $I_M$ . Furthermore, the dominant phase-escape mechanism in a SQUID can be tuned between MQT and PD via a magnetic flux, affecting the SQUID switching current and its standard deviation. This intricate physics is relevant for realizing gate-tunable quantum devices and investigating topological phenomena, where hybrid JJs with phase control are widespread.

We are grateful to C. Müller and W. Riess for helpful discussions. We thank the Cleanroom Operations Team of the Binnig and Rohrer Nanotechnology Center (BRNC) for their help and support. F.N. acknowledges support from the European Research Council (Grant No. 804273) and the Swiss National Science Foundation (Grant No. 200021\_201082). W.B. acknowledges support from the European Union's Horizon 2020 FET Open programme (Grant No. 964398) and from the Deutsche Forschungsgemeinschaft (DFG; German Research Foundation) via the SFB 1432 (ID 425217212).

\*fni@zurich.ibm.com

- [1] P. Krogstrup, N.L.B. Ziino, W. Chang, S.M. Albrecht, M.H. Madsen, E. Johnson, J. Nygård, C. Marcus, and T.S. Jespersen, *Nat. Mater.* **14**, 400 (2015).
- [2] W. Chang, S.M. Albrecht, T.S. Jespersen, F. Kuemmeth, P. Krogstrup, J. Nygård, and C.M. Marcus, *Nat. Nanotechnol.* **10**, 232 (2015).
- [3] J. Shabani, M. Kjaergaard, H.J. Suominen, Y. Kim, F. Nichele, K. Pakrouski, T. Stankevic, R.M. Lutchyn, P. Krogstrup, R. Feidenhans'l, S. Kraemer, C. Nayak, M. Troyer, C.M. Marcus, and C.J. Palmstrøm, *Phys. Rev. B* **93**, 155402 (2016).
- [4] F. Vigneau, R. Mizokuchi, D.C. Zanuz, X. Huang, S. Tan, R. Maurand, S. Frolov, A. Sammak, G. Scappucci, F. Lefloch, and S. De Franceschi, *Nano Lett.* **19**, 1023 (2019).
- [5] C.M. Moehle, C.T. Ke, Q. Wang, C. Thomas, D. Xiao, S. Karwal, M. Lodari, V. van de Kerkhof, R. Termaat, G.C. Gardner, G. Scappucci, M.J. Manfra, and S. Goswami, *Nano Lett.* **21**, 9990 (2021).
- [6] P. Perla, H.A. Fonseka, P. Zellekens, R. Deacon, Y. Han, J. Kölzer, T. Mörstedt, B. Bennemann, A. Espiari, K. Ishibashi, D. Grützmacher, A.M. Sanchez, M.I. Lepsa, and T. Schäpers, *Nanoscale Adv.* **3**, 1413 (2021).
- [7] T. Kanne, M. Marnauza, D. Olsteins, D.J. Carrad, J.E. Sestoft, J. de Bruijkere, L. Zeng, E. Johnson, E. Olsson, K. Grove-Rasmussen, and J. Nygård, *Nat. Nanotechnol.* **16**, 776 (2021).
- [8] M. Pendharkar, B. Zhang, H. Wu, A. Zarassi, P. Zhang, C.P. Dempsey, J.S. Lee, S.D. Harrington, G. Badawy, S. Gazibegovic, R.L.M. Op het Veld, M. Rossi, J. Jung, A.-H. Chen, M.A. Verheijen, M. Hocevar, E.P.A.M. Bakkers, C.J. Palmstrøm, and S.M. Frolov, *Science* **372**, 508 (2021).
- [9] K. Aggarwal, A. Hofmann, D. Jirovec, I. Prieto, A. Sammak, M. Botifoll, S. Martí-Sánchez, M. Veldhorst, J. Arbiol, G. Scappucci, J. Danon, and G. Katsaros, *Phys. Rev. Res.* **3**, L022005 (2021).
- [10] T.W. Larsen, K.D. Petersson, F. Kuemmeth, T.S. Jespersen, P. Krogstrup, J. Nygård, and C.M. Marcus, *Phys. Rev. Lett.* **115**, 127001 (2015).
- [11] L. Casparis, M.R. Connolly, M. Kjaergaard, N.J. Pearson, A. Kringhøj, T.W. Larsen, F. Kuemmeth, T. Wang, C. Thomas, S. Gronin, G.C. Gardner, M.J. Manfra, C.M. Marcus, and K.D. Petersson, *Nat. Nanotechnol.* **13**, 915 (2018).
- [12] C. Janvier, L. Tosi, L. Bretheau, Ç. Girit, M. Stern, P. Bertet, P. Joyez, D. Vion, D. Esteve, M. Goffman *et al.*, *Science* **349**, 1199 (2015).
- [13] G. de Lange, B. van Heck, A. Bruno, D.J. van Woerkom, A. Geresdi, S.R. Plissard, E.P.A.M. Bakkers, A.R. Akhmerov, and L. DiCarlo, *Phys. Rev. Lett.* **115**, 127002 (2015).
- [14] M. Pita-Vidal, A. Bargerbos, C.-K. Yang, D.J. van Woerkom, W. Pfaff, N. Haider, P. Krogstrup, L.P. Kouwenhoven, G. de Lange, and A. Kou, *Phys. Rev. Appl.* **14**, 064038 (2020).
- [15] J.I.-J. Wang, D. Rodan-Legrain, L. Bretheau, D.L. Campbell, B. Kannan, D. Kim, M. Kjaergaard, P. Krantz, G.O. Samach, F. Yan, J.L. Yoder, K. Watanabe, T. Taniguchi, T.P. Orlando, S. Gustavsson, P. Jarillo-Herrero, and W.D. Oliver, *Nat. Nanotechnol.* **14**, 120 (2019).
- [16] M. Hays, V. Fatemi, D. Bouman, J. Cerrillo, S. Diamond, K. Serniak, T. Connolly, P. Krogstrup, J. Nygård, A.L. Yeyati, A. Geresdi, and M.H. Devoret, *Science* **373**, 430 (2021).
- [17] S. Hart, H. Ren, M. Kosowsky, G. Ben-Shach, P. Leubner, C. Brüne, H. Buhmann, L.W. Molenkamp, B.I. Halperin, and A. Yacoby, *Nat. Phys.* **13**, 87 (2017).
- [18] W. Mayer, M.C. Dartiailh, J. Yuan, K.S. Wickramasinghe, E. Rossi, and J. Shabani, *Nat. Commun.* **11**, 212 (2020).
- [19] C. Baumgartner, L. Fuchs, A. Costa, S. Reinhardt, S. Gronin, G.C. Gardner, T. Lindemann, M.J. Manfra, P.E. Faria Junior, D. Kochan, J. Fabian, N. Paradiso, and C. Strunk, *Nat. Nanotechnol.* **17**, 39 (2022).
- [20] M. Hell, M. Leijnse, and K. Flensberg, *Phys. Rev. Lett.* **118**, 107701 (2017).
- [21] F. Pientka, A. Keselman, E. Berg, A. Yacoby, A. Stern, and B.I. Halperin, *Phys. Rev. X* **7**, 021032 (2017).
- [22] A. Fornieri, A.M. Whiticar, F. Setiawan, E. Portolés, A.C.C. Drachmann, A. Keselman, S. Gronin, C. Thomas, T. Wang, R. Kallaher, G.C. Gardner, E. Berg, M.J. Manfra, A. Stern, C.M. Marcus, and F. Nichele, *Nature (London)* **569**, 89 (2019).

- [23] H. Ren, F. Pientka, S. Hart, A. T. Pierce, M. Kosowsky, L. Lunczer, R. Schlereth, B. Scharf, E. M. Hankiewicz, L. W. Molenkamp, B. I. Halperin, and A. Yacoby, *Nature (London)* **569**, 93 (2019).
- [24] M. C. Dartiailh, W. Mayer, J. Yuan, K. S. Wickramasinghe, A. Matos-Abiague, I. Žutić, and J. Shabani, *Phys. Rev. Lett.* **126**, 036802 (2021).
- [25] A. Banerjee, O. Lesser, M. A. Rahman, H. R. Wang, M. R. Li, A. Kringhøj, A. M. Whiticar, A. C. C. Drachmann, C. Thomas, T. Wang, M. J. Manfra, E. Berg, Y. Oreg, A. Stern, and C. M. Marcus, [arXiv:2201.03453](https://arxiv.org/abs/2201.03453).
- [26] F. Nichele, E. Portolés, A. Fornieri, A. M. Whiticar, A. C. C. Drachmann, S. Gronin, T. Wang, G. C. Gardner, C. Thomas, A. T. Hatke, M. J. Manfra, and C. M. Marcus, *Phys. Rev. Lett.* **124**, 226801 (2020).
- [27] H. J. Suominen, J. Danon, M. Kjaergaard, K. Flensberg, J. Shabani, C. J. Palmstrøm, F. Nichele, and C. M. Marcus, *Phys. Rev. B* **95**, 035307 (2017).
- [28] T. A. Fulton and L. N. Dunkleberger, *Phys. Rev. B* **9**, 4760 (1974).
- [29] J. M. Martinis, M. H. Devoret, and J. Clarke, *Phys. Rev. B* **35**, 4682 (1987).
- [30] G.-H. Lee, D. Jeong, J.-H. Choi, Y.-J. Doh, and H.-J. Lee, *Phys. Rev. Lett.* **107**, 146605 (2011).
- [31] A. Murphy, P. Weinberg, T. Aref, U. C. Coskun, V. Vakaryuk, A. Levchenko, and A. Bezryadin, *Phys. Rev. Lett.* **110**, 247001 (2013).
- [32] B.-K. Kim and Y.-J. Doh, *J. Korean Phys. Soc.* **69**, 349 (2016).
- [33] J. Kim, B.-K. Kim, H.-S. Kim, A. Hwang, B. Kim, and Y.-J. Doh, *Nano Lett.* **17**, 6997 (2017).
- [34] M. Sahu, M.-H. Bae, A. Rogachev, D. Pekker, T.-C. Wei, N. Shah, P. M. Goldbart, and A. Bezryadin, *Nat. Phys.* **5**, 503 (2009).
- [35] P. Li, P. M. Wu, Y. Bomze, I. V. Borzenets, G. Finkelstein, and A. M. Chang, *Phys. Rev. Lett.* **107**, 137004 (2011).
- [36] T. Aref, A. Levchenko, V. Vakaryuk, and A. Bezryadin, *Phys. Rev. B* **86**, 024507 (2012).
- [37] V. Lefevre-Seguín, E. Turlot, C. Urbina, D. Esteve, and M. H. Devoret, *Phys. Rev. B* **46**, 5507 (1992).
- [38] S.-X. Li, Y. Yu, Y. Zhang, W. Qiu, S. Han, and Z. Wang, *Phys. Rev. Lett.* **89**, 098301 (2002).
- [39] F. Balestro, J. Claudon, J. P. Pekola, and O. Buisson, *Phys. Rev. Lett.* **91**, 158301 (2003).
- [40] D. F. Sullivan, S. K. Dutta, M. Dreyer, M. A. Gubrud, A. Roychowdhury, J. R. Anderson, C. J. Lobb, and F. C. Wellstood, *J. Appl. Phys.* **113**, 183905 (2013).
- [41] S. Butz, A. K. Feofanov, K. G. Fedorov, H. Rotzinger, A. U. Thomann, B. Mackrodt, R. Dolata, V. B. Geshkenbein, G. Blatter, and A. V. Ustinov, *Phys. Rev. Lett.* **113**, 247005 (2014).
- [42] A. Bezryadin, Stochastic premature switching and Kurki-järvi theory, in *Superconductivity in Nanowires* (John Wiley & Sons, Ltd, New York, 2012), Chap. 8, pp. 131–162.
- [43] L. Longobardi, D. Massarotti, D. Stornaiuolo, L. Galletti, G. Rotoli, F. Lombardi, and F. Tafuri, *Phys. Rev. Lett.* **109**, 050601 (2012).
- [44] See Supplemental Material at <http://link.aps.org/supplemental/10.1103/PhysRevLett.130.087002> for a detailed discussion of the Monte Carlo simulation and for additional experimental results, which includes Refs. [45–50].
- [45] D. Massarotti, L. Longobardi, L. Galletti, D. Stornaiuolo, D. Montemurro, G. Pepe, G. Rotoli, A. Barone, and F. Tafuri, *Low Temp. Phys.* **38**, 263 (2012).
- [46] C. R. Paul, *Analysis of Multiconductor Transmission Lines* (Wiley-IEEE Press, New York, 2008), pp. 160–239, Chap. 5.
- [47] M. H. Devoret, J. M. Martinis, and J. Clarke, *Phys. Rev. Lett.* **55**, 1908.
- [48] R. L. Kautz and J. M. Martinis, *Phys. Rev. B* **42**, 9903 (1990).
- [49] K. Gloos and F. Anders, *J. Low Temp. Phys.* **116**, 21 (1999).
- [50] A. A. Golubov, M. Y. Kupriyanov, and E. Il'ichev, *Rev. Mod. Phys.* **76**, 411 (2004).
- [51] J. C. Fenton and P. A. Warburton, *Phys. Rev. B* **78**, 054526 (2008).
- [52] L. Longobardi, D. Massarotti, G. Rotoli, D. Stornaiuolo, G. Papari, A. Kawakami, G. Piero Pepe, A. Barone, and F. Tafuri, *Appl. Phys. Lett.* **99**, 062510 (2011).
- [53] L. Longobardi, D. Massarotti, G. Rotoli, D. Stornaiuolo, G. Papari, A. Kawakami, G. P. Pepe, A. Barone, and F. Tafuri, *Phys. Rev. B* **84**, 184504 (2011).
- [54] J. M. Martinis and R. L. Kautz, *Phys. Rev. Lett.* **63**, 1507 (1989).
- [55] M. Iansiti, A. T. Johnson, W. F. Smith, H. Rogalla, C. J. Lobb, and M. Tinkham, *Phys. Rev. Lett.* **59**, 489 (1987).
- [56] M. Iansiti, M. Tinkham, A. T. Johnson, W. F. Smith, and C. J. Lobb, *Phys. Rev. B* **39**, 6465 (1989).
- [57] Each SPD was obtained by recording 5,000 switching events.
- [58] C. W. J. Beenakker and H. van Houten, *Phys. Rev. Lett.* **66**, 3056 (1991).